Journal of Solid State Chemistry **163,** 472–478 (2002)
doi:10.1006/jssc.2001.9430, available online at http://www.idealibrary.com on IDEAL®

New $La_{2/3}TiO_3$ Derivatives: Structure and Impedance Spectroscopy

Ana Isabel Ruiz,[1] María Luisa López, Carlos Pico, and María Luisa Veiga

Departamento Química Inorgánica I, Facultad de Ciencias Químicas, Universidad Complutense, 28040 Madrid, Spain

Received June 6, 2001; in revised form October 2, 2001; accepted October 15, 2001

New phases which arise from inserting Na cations on the vacant *A*-sites of the compound $La_{2/3}TiO_3$ have been obtained, giving rise to the series $La_{4/3-x}Na_{3x}Ti_2O_6$ (for $x = 0.16$ and 0.28). These phases adopt a perovskite-type structure as deduced from their characterization by electron microscopy and neutron diffraction. Rietveld analyses show that the symmetry is orthorhombic (S.G. *Ibmm*). Electrical conductivity was determined by impedance spectroscopy, as a function of temperature. A similar behavior is observed for both samples, which behave as ionic conductors with activation energies of 0.92(3) and 0.92(5) eV, respectively. © 2002 Elsevier Science (USA)

Key Words: **perovskite-type structure; neutron diffraction; electron diffraction; ionic conductivity.**

INTRODUCTION

The perovskite structure ABO_3 is adopted by a great number of oxides comprised of *A* and *B* cations with different oxidation states. Their electrical and magnetic properties make them attractive materials for important applications, including high-temperature superconductors, ferro- and piezoelectric, magnetoresistors, semiconductors, sensors, oxygen ion or cationic conductors, cathode materials, etc.

There has been renewed interest in perovskite-type metal oxides of the first transition series with the small number of *d* electrons, e.g. d^1 and d^2 configurations. The system $LaTiO_3$ and related d^1 metal perovskites are of particular interest because the oxidation to $LaTiO_{3+x}$ or $La_{1-x}TiO_3$ (1, 2) varies the titatium formal oxidation state and the concomitant electrical and magnetic properties with respect to the parent oxide. Having in mind that an ABO_3 perovskite structure is constructed from close-packed layers of AO_3 with *B* cations located on one-quarter of the octahedral sites, without vacancies available to be occupied by interstitial oxide anions, the more reasonable formulation for the oxidized species is $La_{1-x}TiO_3$ (3), instead of the alternative $LaTiO_{3+x}$. Thus, a proportion of La^{3+} vacancies appears in the *A*-sites, as a function of the *x* value, the orthorhombic perovskite structure being retained. The higher oxidation state for titanium (Ti^{4+}, d^0) is achieved in the grossly La-deficient compound, formulated as $La_{2/3}TiO_3$.

It has been established that the $La_{1-x}TiO_3$ exists for the full range of compositions, $0.0 \le x \le 0.33$, and in all cases the orthorhombic unit cell parameters are related to the parent cubic perovskite one, a_c (~ 3.8 Å), as follows: $a \approx b \approx a_c\sqrt{2}$, $c \approx 2a_c$. At least three symmetries are involved for different composition ranges (3): *Pnma* ($x = 0.0$–0.12), *Imma* ($x = 0.20$–0.25), and *Pban* ($x = 0.30$–0.33). On the other hand, Kim *et al.* (4) have described two new phases $La_{2/3+x}TiO_{3-\delta}$ as orthorhombic (S.G. *Pmmm*, for $\delta = 0.03$) and tetragonal (S.G. *P*4/*mmm*, for $\delta = 0.13$) showing the structural changes associated with the oxygen deficiency δ and temperature.

Simultaneously, the electrical conductivity measurements on these perovskites have been carried out, showing interesting metal–insulator transitions correlated with the above structural changes. $La_{2/3}TiO_3$ is an insulator and there is a clear progression to metallic behavior as Ti(IV) is reduced, the phase $La_{0.70}TiO_3$ being a semiconductor at room temperature. These electrical properties in the $La_{1-x}TiO_3$ series seem to be related with the Ti^{3+} concentration (3) and a broad metallic range appears between 24% to 94% Ti^{3+}. In the system $La_{2/3+x}TiO_{3-\delta}$ the slightly doped samples show semiconducting behavior, while the heavily doped samples show metallic conductivity.

Another way to modify structural and electrical properties is achieved by introducing alkaline cations in the $La_{2/3}TiO_3$ structure. For instance, lithium cations occupy the vacant *A*-sites and replace some proportion of lanthanum in order to preserve the crystal electroneutrality (5–11), giving rise to the series of perovskites $La_{1.33-x}Li_{3x}Ti_2O_6$. From the structural point of view the new phases adopted a tetragonal symmetry (S.G. *P*4/*mmm*) as was deduced from neutron diffraction experiments (12). Further alkali derivatives $La_{1.33-x}M_{3x}Ti_2O_6$ (M = Li, Na, K)

[1]To whom correspondence should be addressed. E-mail: anairuiz@quim.ucm.es.

0022-4596/02 $35.00

have been reported (13) for which tetragonal (S.G. *P*4/*mmm*) and orthorhombic (S.G. *Pbnm*) symmetries were characterized. For lower sodium content ($x \leq 0.16$) tetragonal phases were obtained and the remaining compositions of sodium and potassium derivatives were orthorhombic (whose parameters a_o, b_o, and c_o are related to the primitive perovskite cell, a_p, as follows: $a_o \approx b_o \approx a_p\sqrt{2}$, $c_o \approx 2a_p$).

The aim of this paper is to establish the crystal structure and electrical behavior of some new phases of the solid solution $La_{1.33-x}Na_{3x}Ti_2O_6$, which arise from inserting Na cations on the vacant *A*-sites of the compound $La_{2/3}TiO_3$, where all *B*-sites are occupied by Ti^{4+}.

EXPERIMENTAL SECTION

Polycrystalline samples of general composition $La_{1.33-x}Na_{3x}Ti_2O_6$ were prepared by the "liquid mix" technique (14) from an aqueous solution of the metal nitrates $La(NO_3)_3 \cdot 6H_2O$, $NaNO_3$, and TiO_2 in stoichiometric ratios. About 4 g of these reagents were added to a mixture of 10 g of citric acid and 4 ml of ethyleneglycol. These ingredients were mixed together and drops of HNO_3 were added to catalyze the gel formation. The excess of nitric acid was boiled off and the gel was slowly decomposed by heating to 400°C. The resulting powders were intimately mixed and heated in several steps up to temperatures ranging between 1273 and 1373 K in air for several days, in platinum crucibles as described elsewhere (15). During the thermal treatment, the samples were reground in each step and the process was monitored by X-ray diffraction until single phases were obtained.

Chemical analyses were performed using inductively coupled plasma (ICP) spectroscopy in a JY-70 apparatus. Samples were dissolved by the digestion with H_2SO_4 and $(NH_4)_2SO_4$.

The neutron powder diffraction data were recorded at room temperature on the D1A high-resolution powder diffractometer ($\lambda = 1.9110$ Å) at the Institut Laue-Langevin (Grenoble, France). Neutron diffraction patterns were analyzed by the Rietveld method and the Fullprof program (16). A pseudo-Voigt function was chosen to generate the lineshape of the diffraction peaks.

Electron diffraction (ED) data and high-resolution electron microscopy (HREM) were carried out on a JEOL 400 EX microscope. Samples were prepared by dispersing ultrasonically small particles in *n*-butanol and disposing drops of this suspension on a carbon-coated copper grid.

Electrical measurements were carried out using a Solartron 1260 impedance/gain phase analyzer with a frequency range of 1 Hz–10 MHz. Samples were pressed into pellets, of 13 mm diameter and 1.9 mm thickness, and then sintered in air between 1223 and 1373 K for 48 h. Blocking electrodes were deposited on two faces of pellets by platinum paint. The painted pellets were heated at 475 K for 2 h and at 1073 for 4 h.

RESULTS AND DISCUSSION

Chemical Composition and Structural Analysis

Chemical analysis gave the metal ratios in these compounds whose resulting compositions were $La_{1.05}Na_{0.84}Ti_2O_6$ ($x = 0.28$) and $La_{1.17}Na_{0.48}Ti_2O_6$ ($x = 0.16$).

ED patterns along the $[\bar{1}10]_p$ zone axis (Figs. 1a and 1b) were indexed for both samples on the basis of a single cubic perovskite and showed the existence of extra reflections indicative of a supercell, whose parameters are $\sqrt{2}a_p \times \sqrt{2}a_p \times 2a_p$ (where a_p is the lattice constant of the ideal perovskite). The microstructures show lattice fringes at 5.5 and 7.8 Å.

Different results were obtained in a related system $La_{2/3-x}Li_{3x}TiO_3$, by optical diffraction experiments that were interpreted assuming a cell size defined by $a_p \times a_p \times 2a_p$ (6). On this basis, the ED pattern should be due to the superposition of those corresponding to three different domains, in which the *c* axis was randomly oriented along the three space directions. A different interpretation of the

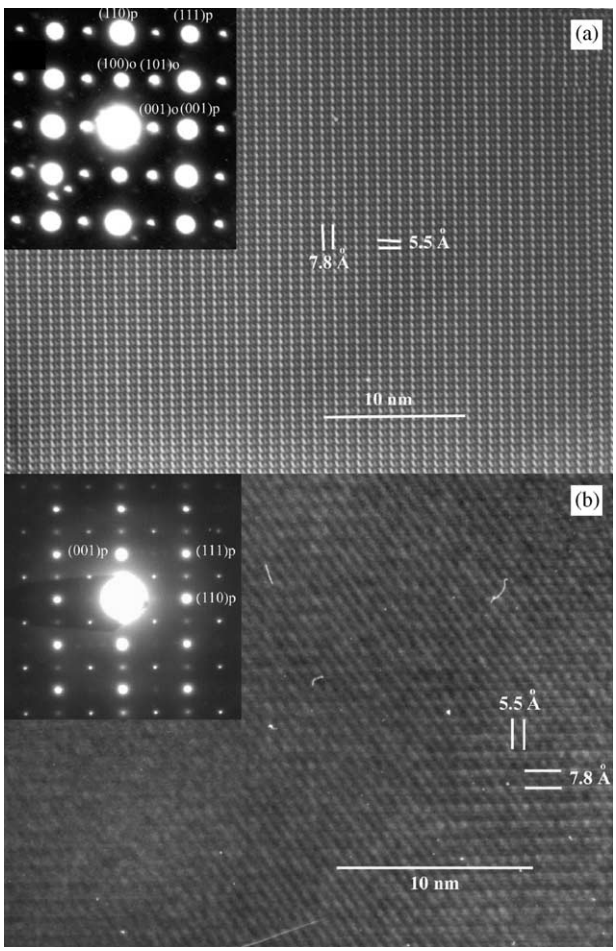

FIG. 1. ED patterns the $[\bar{1}10]$ zone axis and the respective electron micrographs for (a) $La_{1.05}Na_{0.84}Ti_2O_6$ and (b) $La_{1.17}Na_{0.48}Ti_2O_6$.

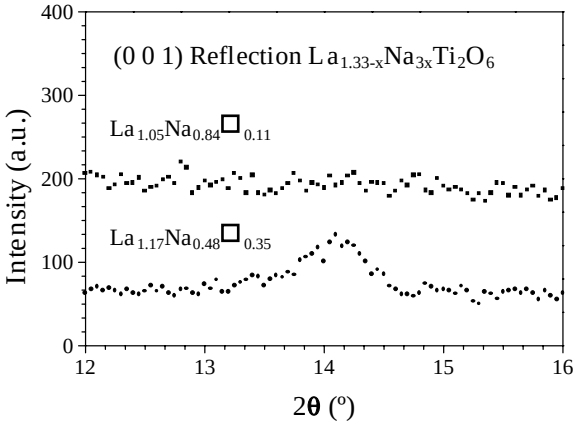

FIG. 2. The (001) reflection in $La_{1.17}Na_{0.48}Ti_2O_6$ and $La_{1.05}Na_{0.84}Ti_2O_6$ (*Ibmm*).

ED pattern was proposed for the phase $La_{0.5}Li_{0.5}TiO_3$ (17), by considering a cell given by $\sqrt{2}a_p \times \sqrt{2}a_p \times 2a_p$, that implies an ordering between lanthanum and lithium in a diagonal cell that should be responsible for the observed cross-shaped diffuse spots along the $[100]_p$ and $[010]_p$ directions.

However, in our system, where the perovskite *A*-sites are partially occupied by Na^+ ions, both ED and HREM results suggest the adoption of an orthorhombic superstructure that seems to be influenced by the greater radius of the alkaline cation.

In order to confirm the above superstructure model, a study by neutron diffraction has been carried out. Some differences are clearly observed as a function of the alkaline metal content, *x*. Main diffraction lines remain unchanged, but the (001) reflection arises when *x* decreases (Fig. 2).

This occurs also in the similar systems $La_{1-x}TiO_3$, where the first member of this series (3) ($x = 0.33$) adopts the *Pban* space group, which is also found for intermediate compositions in the system $La_xSr_{(1-3x)/2}TiO_3$ (18).

The structure determination for $La_{1.17}Na_{0.48}Ti_2O_6$ was not straightforward. First, the *Pban* space group solution was attempted, but the results were not satisfactory. Inspection of the fitted profiles revealed that the intensity distribution was not consistent between the ND data and the space group and very high *R*-factors were obtained. Therefore, the *Pban* space group must be excluded in our system. On the other hand, a close examination of the profile revealed the presence of extra reflections that could not be taken into account for any supercell. This phase was present in a very low concentration ($\approx 3\%$) and was attributed to TiO_2 (rutile) as impurity and was included in the refinement as a second phase.

Next, the *Ibmm* space group was tried. The observed, calculated, and difference neutron diffraction profiles are shown in Fig. 3a and these results seem to confirm that this material is adequately described in the *Ibmm* space group. The structural parameters and *R*-factors are given in Table 1. However, in Fig. 3a one can observe three small reflections, which are forbidden in the *Ibmm* space group and are marked with asterisks. This fact was observed in the system $La_{1-x}TiO_3$, where the (001) reflection appears in the neutron diffraction profile for the lanthanum content $La_{0.67}$, $La_{0.70}$, and $La_{0.75}$, described the latter as *Ibmm*. In our case, such a reflection, as occurs in $La_{0.75}TiO_3$, is very broad (see Fig. 2). This may indicate the presence of small domains with a local structure similar to the *Pban* structure within an overall *Ibmm* long-range order (3).

Refinement of the second sample, $La_{1.05}Na_{0.84}Ti_2O_6$ ($x = 0.28$), by neutron data was successful in *Ibmm*. All the observed diffraction peaks could be indexed in the orthorhombic *Ibmm* space group (see Table 1). The observed, calculated, and difference profiles of this phase are plotted in Fig. 3b. The successive refinements converge to give the final agreement factors that are indicative of a reliable structural model.

The atomic coordinates as well as the isotropic temperature factors obtained are also given in Table 1. Selected interatomic distances show a regular 6-coordination for Ti, therefore located on the *B*-perovskite sites, as well as a quite distorted 12-coordinated polyhedron for La and Na (both on the *A*-sites). Mean bond distances are close to those obtained by the ionic radii sums (19).

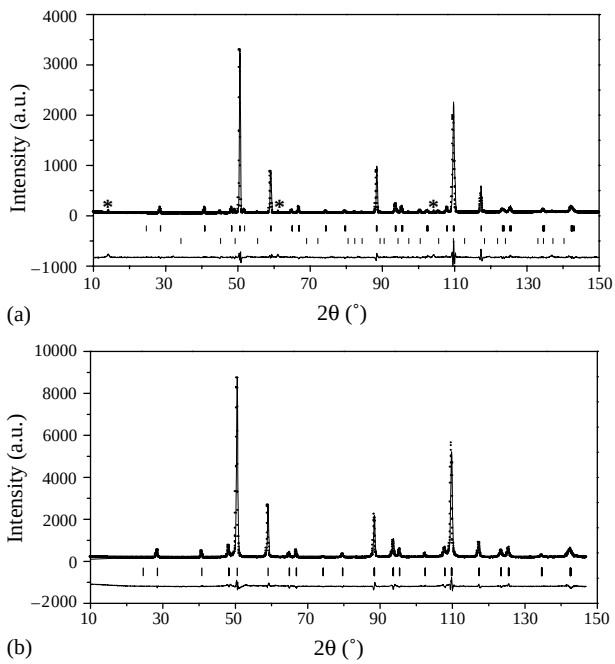

FIG. 3. Calculated (line) and observed (dots) ND patterns and difference spectrum for (a) $La_{1.17}Na_{0.48}Ti_2O_6$ (1, orthorhombic phase; 2, TiO_2 rutile; *, superstructure lines); (b) $La_{1.05}Na_{0.84}Ti_2O_6$ (orthorhombic phase).

TABLE 1
Refined Atomic Positions, Isotropic Temperature Factors (in Å^2), Cell Constants (in Å), and Selected Interatomic Distances (in Å) for $La_{1.33-x}Na_{3x}Ti_2O_6$ ($x = 0.16$, 0.28)

		$x = 0.16$	$x = 0.28$
S.G.		*Ibmm*	*Ibmm*
La/Na	x	0.0030(4)	0.0019(1)
	y	0.0000	0.0000
	z	0.2500	0.2500
	β	0.25(3)	0.97(4)
Ti	x	0.0000	0.0000
	y	0.5000	0.5000
	z	0.0000	0.0000
	β	0.66(4)	0.82(8)
O1	x	0.0385(2)	0.0452(2)
	y	0.5000	0.5000
	z	0.2500	0.2500
	β	1.21(2)	1.52(1)
O2	x	0.7500	0.7500
	y	0.2500	0.2500
	z	0.0009(4)	0.0238(5)
	β	0.94(2)	1.38(7)
a		5.4859(7)	5.4798(2)
b		5.4841(1)	5.4753(4)
c		7.7352(1)	7.7432(5)
R_B		4.89	5.29
R_P		9.03	6.20
R_{WP}		12.1	7.82
d(La/Na–O1)		2.515(2)	2.482(5)
		2.750(8) ($\times 2$)	2.748(1) ($\times 2$)
		2.971(1)	2.998(3)
d(La/Na–O2)		2.667(5) ($\times 4$)	2.617(3) ($\times 4$)
		2.814(1) ($\times 4$)	2.866(8) ($\times 4$)
Mean		2.742	2.742
Shannon		2.77	2.77
d(Ti–O1)		1.945(8) ($\times 2$)	1.952(2) ($\times 2$)
d(Ti–O2)		1.944(2) ($\times 4$)	1.945(6) ($\times 4$)
Mean		1.944	1.947
Shannon		2.00	2.00

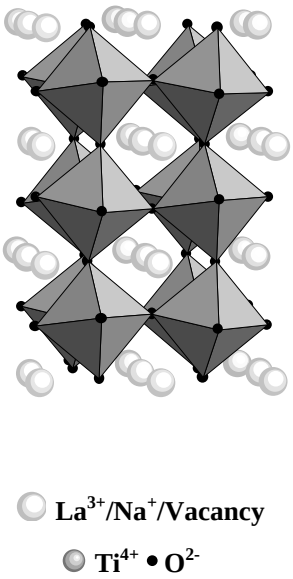

FIG. 4. Structural model of orthorhombic symmetry (S.G. *Ibmm*).

In summary, these samples possess a perovskite-type structure that is built up by TiO_6 octahedra which show very small tilting angles, about two of three orthogonal subcell axes (Fig. 4), following Glazer's octahedra tilt scheme (20), as is deduced from the a/b parameters ratio ($a/b = 0.9997$ for $x = 0.16$ and $a/b = 0.9992$ for $x = 0.28$). Finally, vacancies as well as Na^+ and La^{3+} cations in higher coordination sites are distributed at random.

Electrical Properties

Having in mind that the starting point to understand the transport properties is the previous knowledge of the crystal structure of the material, the above structural results suggested that these phases can behave as ionic conductors, because of the wide range in the number of vacant A-sites and their accessibility by the mobile Na^+ cations.

Electrical characteristics of ionic materials are often studied by a.c. techniques to avoid the necessity of developing the nonblocking ion-conducting electrodes that are needed for d.c. measurements (21, 22).

Complex impedance (Z) diagrams (23) are shown in Fig. 5 for $x = 0.16$ at three different temperatures. The impedance spectra obtained are very similar and they are clearly depressed below the baseline, which is a consequence of the universal response of these materials (24). An equivalent circuit composed of an RC and a constant phase element, CPE (25), has been used to fit the experimental data. The

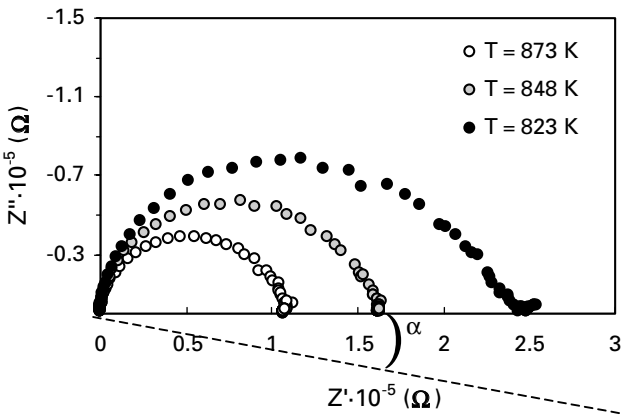

FIG. 5. Complex impedance plots at various temperatures for $La_{1.17}Na_{0.48}Ti_2O_6$.

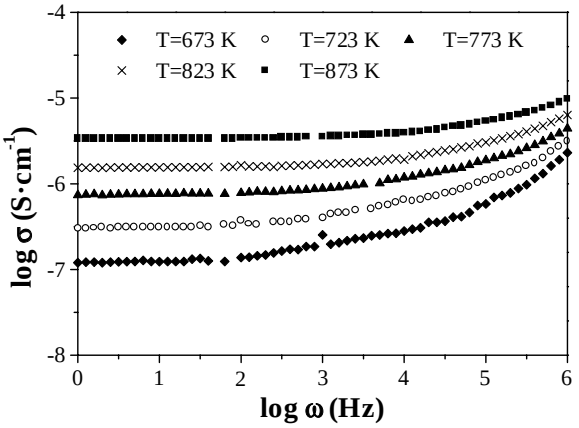

FIG. 6. Plots of log conductivity vs log frequency at different temperatures for $La_{1.17}Na_{0.48}Ti_2O_6$.

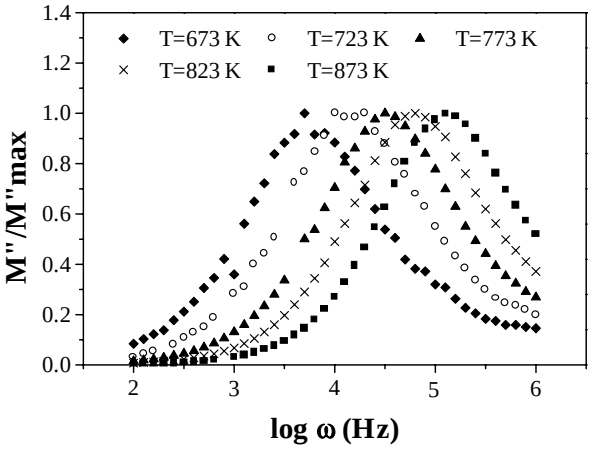

FIG. 7. Modulus (M'') spectra at various temperatures for $La_{1.17}Na_{0.48}Ti_2O_6$.

magnitudes of the capacitance are in the range between 7 and 21 pF, and these values indicate a bulk boundary response.

The frequency dependence of the real part of the conductivity is given in Fig. 6. The conductivity shows a low-frequency plateau corresponding to the d.c. conductivity. At higher frequencies, the conductivity increases as a power law. This frequency dependence can be described by (26, 27) $\sigma(\omega) = \sigma_o + A\omega^n$, where σ_o is a d.c. term, A is a temperature-dependent parameter, and n is the slope of the highest frequencies. The term ω_p is a crossover frequency at which the conductivity starts to follow a power law and is proportional to the ion-hopping rate (28, 29). The n exponent falls in the range $0.6 < n < 1$ at lower temperatures and is often identified with the hopping-type ionic conductors, that is, with the degree of correlation among moving ions.

In addition, the real and imaginary parts of complex electric modulus ($M^* = M' + iM''$) have been calculated at various frequencies and temperatures using the relation $M^*(\omega) = i\omega\varepsilon_o Z^*(\omega)$. Typical plots of M'' for $La_{1.17}Na_{0.48}Ti_2O_6$ are shown in Fig. 7. Only one maximum appears and this fact suggests that the system can be represented by a single parallel RC element (30). A non-Debye-type behavior of electrical relaxation which has also been found earlier in other systems (22) is evident from the large width of the peak (see Fig. 7). Conductivity relaxation times, $\tau_s = 1/F_p$, can be calculated from the frequency peaks, F_p, at different temperatures.

The values obtained for F_p (related to relaxation times) and ω_p (related to ion-hopping rate) indicate that they are dependent on the temperature. Figure 8 shows the variations of F_p, ω_p, and σ_o vs $1000/T$ for the $x = 0.16$ phase. The parallel lines indicate that both quantities, F_p and ω_p, are thermally activated and they have the same activation energy. This fact suggests that the conductivity dispersions observed in log σ seem to be due to the hopping motion of the alkaline cations. Therefore, one can exclude a localized dielectric loss, as well as other electrode or interfacial polarization effects. Similar results were obtained for the $x = 0.28$ sample.

Ionic conductivity values were analyzed by an Arrhenius equation, $\sigma T = \sigma_o \exp(-E_a/kT)$, where σ_o and E_a represent the pre-exponential factor and the activation energies, respectively. Figure 9 shows the linear plots of log σT vs $1000/T$ for two compositions, with very similar activation energies in both cases. The conduction pathway proposed is given in Fig. 10. This mechanism implies that the Na^+ ions must move through square windows in the structure, whose O–O distances are about 3.90 Å. Recently, we reported the conductivity of $La_{1.33-x}Li_{3x}Ti_2O_6$ (10), for which the obtained results are related to the number of mobile monovalent ions and vacancies in the A-sites. Between these high coordination sites there are the square windows whose dimensions are in the limit to allow Li ions move across the diagonal; in this case O–O distances should be higher than

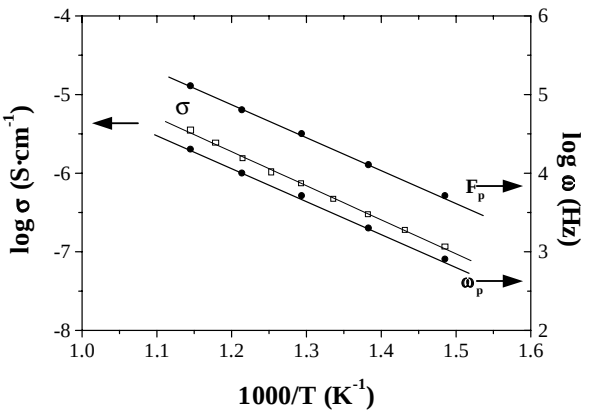

FIG. 8. Temperature dependence of conductivity, σ, inverse relaxation times ($\tau_s^{-1} = F_p$), and ω_p frequency for $La_{1.17}Na_{0.48}Ti_2O_6$.

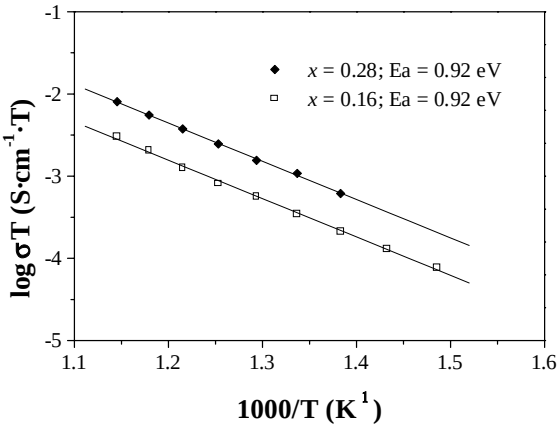

FIG. 9. Arrhenius plots for the system $La_{1.33-x}Na_{3x}Ti_2O_6$.

3.96 Å, corresponding to Li in a planar 4-fold coordination (31). Therefore, the activation energy values obtained for these compounds were low. By contrast, in the Na^+ series, these hindrances will increase due to the greater size of Na^+ with respect to Li^+. Effectively, the activation energies for these phases are double those for the Li^+ ones. This fact seems to indicate that these values depend on the ion mobility through the crystal structure and these high values of the activation energies are due to the mobility restrictions for Na^+ throughout the conduction pathway.

On the other hand, by comparing the lithium and sodium series, a higher conductivity and a lower activation energy were found for $Li_{0.62}La_{1.12}Ti_2O_6$, where the ratio between carriers and vacancies is the most adequate. By contrast, in the Na compounds, a similar behavior in the conductivity and activation energies for both samples are obtained. For the composition given by $x = 0.28$ the number of carriers is high and there is a relatively low number of vacant sites (~ 0.11) to which they can move whereas for the $x = 0.16$ compound, the opposite situation is presented, i.e., the number of carriers is lower but the concentration of vacant sites is higher (~ 0.35). Having in mind both factors and the above similar behavior, we can conclude that the limiting factor would be the bottleneck effect defined by four adjacent TiO_6 octahedra.

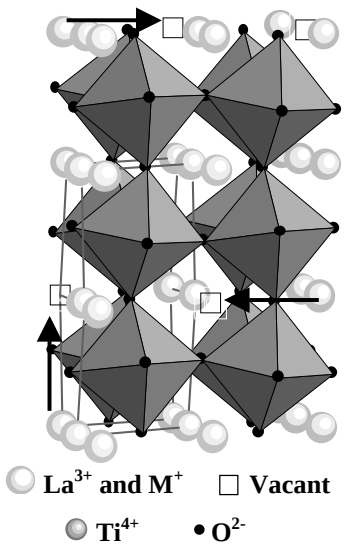

FIG. 10. Pathway conduction for $La_{1.33-x}M_{3x}Ti_2O_6$.

ACKNOWLEDGMENTS

A.I.R. is grateful to the C.A.M. for a fellowship. We are indebted to the CICYT (MAT 2000-1585-C03-02), Spain, for financial support. We acknowledge the I.L.L. for collecting data of Neutron Diffraction and to Dr. M. T. Fernández-Díaz for comments. We also thank the C.A.I. of Espectrometría Atómica, X-Ray Diffraction and Microscopía Electrónica "Luis Bru" from U.C.M. for their technical assistance.

REFERENCES

1. I. Okada, T. Arima, I. Tokura, C. Murayama, and N. Môri, *Phys. Rev. B* **48,** 9677 (1993).
2. D. A. Crandles, T. Timusk, J. D. Garrett, and J. E. Greedan, *Phys. Rev. B* **49,** 16207 (1994).
3. M. J. MacEarchern, H. Dabkowska, J. D. Garrett, G. Amow, W. Gong, G. Liu, and J. E. Greedan, *Chem. Mater.* **6,** 2092 (1994).
4. I. S. Kim, T. Nakamura, Y. Inaguma, and M. Itoh, *J. Solid State Chem.* **113,** 281 (1994).
5. H. Kawai and J. Kuwano, *J. Electrochem. Soc.* **141**(7), L78 (1994).
6. J. L. Fourquet, H. Duroy, and M. P. Crosnier-López, *J. Solid State Chem.* **127,** 83 (1996).
7. C. León, J. Santamaría, M. A. París, J. Sanz, J. Ibarra, and L. M. Torres, *Phys. Rev. B* **56**(9), 5302 (1997).
8. J. Emery, J. Y. Buzare, G. Bonke, and J. L. Fourquet, *Solid State Ionics* **99,** 41 (1997).
9. Y. Inaguma and M. Itoh, *Solid State Ionics* **86–88,** 257 (1996).
10. A. I. Ruiz, M. L. López, M. L. Veiga, and C. Pico, *Solid State Ionics* **112,** 291 (1998).
11. Y. Inaguma, C. Liguan, M. Itoh, T. Nakamura, T. Uchida, H. Ikuta, and M. Wakihara, *Solid State Commun.* **86,** 689 (1993).
12. A. I. Ruiz, M. L. López, M. L. Veiga, and C. Pico, *J. Solid State Chem.* **92,** 110 (1999).
13. A. I. Ruiz, M. L. López, M. L. Veiga, and C. Pico, *Int. J. Inorg. Mater.* **1,** 193 (1999).
14. M. Pechini, U.S. Patent **3,** 231, 328 (1966).
15. I. Alvarez, J. L. Martínez, M. L. Veiga, and C. Pico, *J. Solid State Chem.* **125,** 47 (1996).
16. J. Rodriguez Carvajal, "Fullprof: A program for Rietveld refinement and pattern machine analysis." 1994 (revised version).
17. A. Várez, F. García-Alvarado, E. Morán, and M. A. Alario-Franco, *J. Solid State Chem.* **118,** 78 (1995).
18. P. D. Battle, J. E. Bennett, J. Sloan, R. J. D. Tilley, and J. F. Vente, *J. Solid State Chem.* **149,** 360 (2000).
19. R. D. Shannon, *Acta Crystallogr., Sect. A* **32,** 751 (1976).
20. A. M. Glazer, *Acta Crystallogr., Sect. A* **31,** 756 (1975).
21. R. D. Armstrong, T. Dickinson, and P. M. Willis, *Electroanal. Chem. Interfacial Electrochem.* **53,** 389 (1974).
22. A. K. Jonscher, and J. M. Réau, *J. Mater. Sci.* **13,** 563 (1978).

23. Zview, Graphics and Analysis Software, Scribner Associates, 1994.
24. A. K. Jonscher, "Dielectric Relaxation in Solids." Chelsea Dielectric Press, London, 1983.
25. J. R. MacDonald, "Impedance Spectroscopy. Emphasizing Solid Materials and Systems." Wiley-Interscience, New York, 1987.
26. A. K. Jonscher, *Nature* **267,** 673 (1977).
27. R. M. Hill and A. K. Jonscher, *J. Non-Cryst. Solids* **32,** 53 (1979).
28. D. P. Almond, C. C. Hunter, and A. R. West, *J. Mater. Sci.* **19,** 3236 (1984).
29. D. P. Almond, A. R. West, and R. J. Grant, *Solid State Commun.* **44,** 1277 (1982).
30. M. A. Arillo, M. L. López, C. Pico, and M. L. Veiga, *Solid State Ionics* **120,** 227 (1999).
31. M. A. París, J. Sanz, C. León, J. Santamaría, J. Ibarra, and A. Várez, *Chem. Mater.* **12,** 1694 (2000).